

Research Article

Embedded Connector in Severe Optimization of Steel Plate for Shear Strengthening of RC Beam: Experimental and Numerical Investigations

Md. Ashraful Alam,¹ Suliman A. Bakkar ,² Shahnawaz A. Onik,² and Kamal N. Mustapha²

¹Department of Civil Engineering, University of Asia Pacific, Dhaka, Bangladesh

²Department of Civil Engineering, College of Engineering, Universiti Tenaga Nasional, Selangor, Malaysia

Correspondence should be addressed to Suliman A. Bakkar; sulimanbakkar@hotmail.com

Received 3 August 2017; Accepted 2 April 2018; Published 4 June 2018

Academic Editor: Luigi Di Sarno

Copyright © 2018 Md. Ashraful Alam et al. This is an open access article distributed under the Creative Commons Attribution License, which permits unrestricted use, distribution, and reproduction in any medium, provided the original work is properly cited.

Environmental impact has become one of the major factors taken into consideration for recent civil engineering studies and projects. Thus, researchers have been concentrating on shear strengthening of existing reinforced concrete structure as an upgrade method instead of demolishing and reconstructing. In general, shear strengthening of RC beams using externally bonded steel plate has gained huge popularity. However, premature debonding of plates is the main drawback of the system, which could be mitigated using embedded connector; thus, the dimension of steel plate could be reduced significantly. Furthermore, numerical analysis on shear strengthening of beams using embedded connector would provide a great insight on the structural behavior. The aim of this research is to severely reduce the dimension of the steel plate using embedded connector for shear strengthening of RC beams and to investigate the performances of optimized shear-strengthened beams through experimental and numerical investigations. The results showed that the dimension of plate was reduced without debonding of the plate if the beam was designed for shear strengthening with the consideration of yield strength of steel plate and shear link. Experimental results showed a maximum increase in failure of 24%. The numerical results predicted accurately the structural performance of beams. The embedded connector had a great effect in deferring and minimizing the debonding failure and accordingly increasing the maximum load of shear failure between 14.5% and 24% compared to control beam.

1. Introduction

Normally, RC beams are designed to have a higher shear capacity than flexural capacity, so shear failure can be avoided as it is brittle and sudden in nature. However, multiple causes such as severe corrosion of the steel stirrups due to deterioration or change in loading can lead to lower shear capacity. In addition, flexural strengthening of RC members may cause the shear capacity to be insufficient which is highly unrecommended and shear strengthening would become necessary. In the recent years, upgrading the structural performance of RC structures by strengthening with externally bonded plates has gained an increasing popularity using materials such as steel plates, aluminum alloy plates [1, 2], FRP composites [3–6], and natural fiber

plates. On the other hand, strengthening using steel plates has its advantages, such as cheap and reliable, ease of installing, high tensile modulus, and excellent compatibility with concrete [7]. In addition, the advancement of new materials and technologies has led researchers to investigate various designs and materials to increase the strength of shear critical RC beams [8–14]. Shear strengthening of rectangular RC beams with steel plates can be applied using three different approaches: full wrapping, U-wrapping, and side strips. Side strips are the least effective as it easily debonds from the concrete surface, while full wrapping provides the highest effectiveness followed by U-wrapping. However, side-bonded strips are the most practical to apply where it does not need access to the top or the bottom of the beam. Premature debonding of EB plates is the main weakness of the system

where it is caused by concrete cracks leading to the separation of the adhesive from concrete surface at ends of strengthening plate. Many studies have been done on the side-bonded method over the past two decades [5–7, 15–19]. Numerous materials, arrangements, and anchors have been investigated to increase the shear capacity of the RC member as well as delay the premature debonding failure in externally bonded (EB) members [10, 20–30, 31].

Various anchor designs were proposed to overcome the issue of premature debonding; however, not all can be considered as the perfect solution. El-Saikaly et al. [32] had tested an anchor that consisted of CFRP robes overlapping with CFRP L-strips through drilled holes all the way in the web of the beam simulating fully wrapped mode. The anchor was proved to be effective; however, it imposes a great risk of cutting a shear link while drilling and it requires hard effort for drilling. Chen et al. [33] used different designs to anchor the U-shaped CFRP wraps to holes drilled in the flange of the T-beam. The authors concluded that all designs were effective; nevertheless, this type of anchor can only be used with CFRP sheet. Tetta et al. [34] proposed multiple layers of U-shaped fabrics anchored with single or multiple fan anchors which are drilled into the flange of the beam. Although the method was effective, it is expensive and might cause damage to the flange. Baggio et al. [10] also used fan anchor embedded through the entire section of beam to anchor U-shaped FRP sheets. The test was successful; nevertheless, it risks cutting through the shear link, it requires high labor for drilling, and it can only be used on sheets as it needs to cut through them. On the other hand, embedded connector only requires drilling through the concrete cover and does not cut through the strengthening plate as it is embedded beneath it and it imposes no risk on the shear link or the core of the concrete beam. Previous tests on the shear strengthening were not fully able to eliminate the premature debonding; thus, optimization was not possible. However, as embedded connector was proven to be a reliable technique to eliminate debonding failure, full utilization of the strengthening plate is possible as well as the optimization of its dimension.

Researchers have used many design approaches to obtain the optimal dimensions for the strengthening system. One of the methods is the strut-and-tie or swarm optimization method which is based on the minimization of the error between the measured and predicted results where the problem is solved using particle swarm optimization (PSO) algorithms [35]. Another method is using strain of the strengthening plate to obtain its cross section like what ACI Committee 440 [36] suggests. However, the maximum allowable strain is below the tensile strain of most common materials used for shear strengthening, and thus, the used material is not fully utilized by the strengthening system [37]. Another procedure is using a third term to account for the contribution of the strengthening plate to the shear strength, as follows: $V_r = V_C + V_S + V_P$. In this equation, the shear strength of the section, V_r , is the sum of the shear strength contributions of the concrete (V_C), steel stirrups (V_S), and strengthening plate (V_P). This method is widely used for its simplicity [35, 38].

Recently, finite element analysis has become popular for testing RC beams with different objectives as it provides

accurate results that are comparable to the experimental tests and it allows many variations to the tested model without the hassle of additional actual specimens. Panigrahi [39] tested GFRP shear-strengthened T-beams for the effect of laminate thickness on crack pattern, mode of failure, and strength of RC beams. The model represented the concrete model with cohesive bonded laminates and could predict the experimental results accurately. Baghi and Barros [40], Khan et al. [41], and Lee et al. [42] also tested CFRP shear-strengthened numerical model of T-beams for the load carrying capacity, crack patterns, strain in the CFRP laminates, and failure modes of the tested beams where the model was successful with high accuracy. In addition, the authors used the model for parametric study to predict the effect of shear link reinforcement ratio on beam capacity. Awani et al. [43] also used finite element model to predict the crack pattern, load capacity, load-deflection response, stirrup, and laminate strain response where the model produced accurate predictions. Although many numerical models were produced, little has been done toward modeling mechanical anchor like the embedded connector.

Embedded connector system was introduced in this research, and its effect on the shear capacity of the externally bonded steel plates was investigated as an attempt to provide valuable insight into the general performance of embedded connector system. In addition, optimization of the steel plate width was considered. The study involves performing experiments to understand the mechanical behavior and calibrate and perform a numerical simulation, whose results are seen to be compared with the experimental results to get a better understanding of the experimental system.

2. Design Approach

The maximum shear capacity of a normal RC beam can be calculated according to the moment applied on the beam divided by the shear span as shown in the following equation:

$$V_{\max} = \frac{M_{\max}}{\text{shear span}} \quad (1)$$

However, the shear strength of the beam is represented by concrete shear strength as well as yield strength of the steel link as shown in the following equation:

$$V_{\text{beam}} = V_{\text{concrete}} + V_{\text{link}}, \quad (2)$$

where

$$V_{\text{link}} = 2\pi \frac{\varphi_{\text{link}}^2}{4} f_{\text{link}} \frac{(d - d') \cot \theta}{S_{\text{link}}} \quad (3)$$

Therefore, when $V_{\text{beam}} < V_{\max}$, the beam will fail on shear, and when $V_{\text{beam}} > V_{\max}$, the beam will fail on flexure. However, the loading of the strengthening system begins as concrete cracks start forming at the strengthened area ($V_{\text{concrete}} = 0$).

As beams are designed to fail on shear for the purpose of the strengthening the beams on shear, the tested beams were designed as $V_{\text{beam}} < V_{\max}$, where the design shear capacity

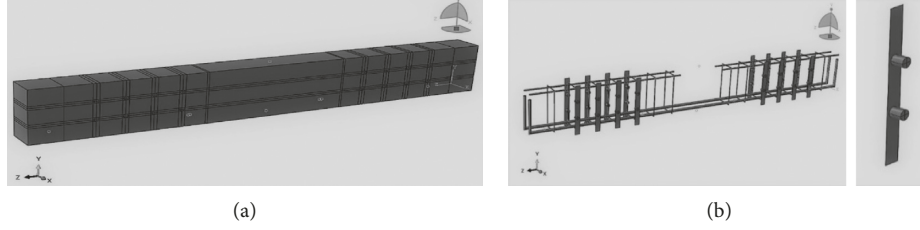


FIGURE 1: Beam modeling in ABAQUS: (a) 3D modeling of beam; (b) rebar, plate, and embedded connector modeling.

(V_{design}) of the beam is as in (4) in order to calculate the optimum design dimension of the steel plate.

$$V_{\text{design}} = V_{\text{max}}, \quad (4)$$

$$V_{\text{design}} = V_{\text{beam}} + V_{\text{plate}}, \quad (5)$$

$$V_{\text{plate}} = V_{\text{max}} - V_{\text{beam}}. \quad (6)$$

There are two main approaches to obtain the dimension of the steel plate: the first one is based on the yield strength of shear link as the beam is expected to fail when both plate and shear link reach yield stress, where

$$V_{\text{link}} = 2\pi \frac{\phi_{\text{link}}^2}{4} f_{y,k,\text{link}} \frac{(d-d') \cot \theta}{S_{\text{link}}}, \quad (7)$$

$$V_{\text{plate}} = 2A_{\text{plate}} f_{y,k,\text{plate}} N, \quad (8)$$

$$V_{\text{plate}} = 2A_{\text{plate}} f_{y,k,\text{plate}} \frac{(d-d') \cot \theta}{S_{\text{plate}}}; \quad \theta = 45^\circ. \quad (9)$$

From (9), we can calculate the required area of the steel plate (A_{plate}):

$$A_{\text{plate}} = \frac{V_{\text{plate}}}{\left[2f_{y,k,\text{plate}} (d-d') \cot 45^\circ / S_{\text{plate}} \right]}. \quad (10)$$

The other approach is based on the tensile strength of shear link where the failure is expected to happen when both steel plate and shear link reach their tensile strength as shown in the following equations:

$$V_{\text{link}} = 2\pi \frac{\phi_{\text{link}}^2}{4} f_{t,k,\text{link}} \frac{(d-d') \cot \theta}{S_{\text{link}}}. \quad (11)$$

Thus, steel plate cross-sectional area (A_{plate}) could be calculated as follows:

$$A_{\text{plate}} = \frac{V_{\text{plate}}}{\left[2f_{t,k,\text{plate}} (d-d') \cot 45^\circ / S_{\text{plate}} \right]}. \quad (12)$$

3. Numerical Modeling in ABAQUS

A three-dimensional nonlinear finite element model was developed using ABAQUS/CAE, which is suitable for materials with degradation and failure such as concrete because its stiffness becomes negative as cracks happen. Several constitutive models were developed and analyzed, and the

most appropriate ones were selected to develop the finite element model based on the obtained results. The modeling procedures used in this research are briefly illustrated in the following subsections.

3.1. Geometric Modeling. Three-dimensional solid elements were employed for the reinforced concrete beam (as shown in Figure 1), as well as the strengthening steel plates which were represented using three-dimensional shell elements (Figure 1). Mesh density was investigated for the model, and a mesh size of 25 mm was chosen in each direction. In addition, the selected mesh size maintains a balance between computational time and accuracy of results.

Embedded steel bars modeled as solid elements were employed to represent the reinforcement bars and shear links of beams (Figure 1(b)). The reinforcement elements were embedded in the concrete using “embedded region” constraint, and its strains are computed from the displacement field of the concrete elements surrounding it. In this study, perfect bond was assumed between the internal steel reinforcement and the surrounding concrete as bond failure had not been observed during the experimental tests [39, 41].

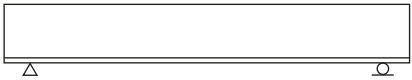
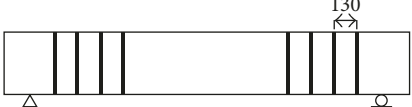
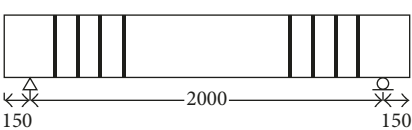
3.2. Material Modeling. A damaged plasticity model for concrete available in ABAQUS/CAE served as the basis for the constitutive model of the reinforced concrete beams. This model uses concepts of isotropic compressive and tensile plasticity in combination with scalar damage to describe irreversible reductions in stiffness during the fracturing process [39, 44]; these values were obtained from the compressive and tensile tests in the laboratory. The elastic modulus and Poisson’s ratio are the two basic parameters to define the elastic mechanical behavior of concrete (elastic modulus is 30 GPa, and Poisson’s ratio is 0.2).

An elastic-perfectly plastic stress-strain model was adopted for the internal steel reinforcement and steel plates, as well as for embedded connectors [39].

3.3. The Bond between Steel Plates and Concrete Surface.

For modeling bond area between the strengthening laminates with the concrete surface of the beam, as well as the embedded connector and the concrete surface, tie constraints were utilized. Tie constraints are used to tie together two surfaces for the duration of a simulation where each node on the slave surface is constrained to have the same motion as the point on the master surface to which it is closest. For a structural

TABLE 1: Details of specimens.

Specimens	Steel plate dimension			Embedded connector diameter (mm)	Design criteria of plate	Beam diagram
	Length (mm)	Width (mm)	Thickness (mm)			
CB	—	—	—	—	—	
BSC20	300	20	2.75	16	Tensile	
BSC25	300	25	2.75	16	Between yield and tensile	
BSC30	300	30	2.75	20	Yield	

analysis, this means the translational degrees of freedom are constrained. In our case, the CFRP laminates and embedded connectors acted as the master surfaces while the concrete surface of the beam acted as the slave surface [39].

3.4. Boundary Conditions and Loading. A mechanical displacement/rotation boundary condition is used in ABAQUS/CAE to model the supports of the RC beams. The beam was designed to be simply supported with one side pinned by restricting its movement on the Y and Z directions and the other side as a roller support by restricting its movement on the Y direction, where the supports are 150 mm from the edge of the beam [45].

Four-point loading is used to produce a flexural failure similar to the experimental tests. A pressure load is used to simulate the two point loads on the RC beams as it is most alike the real loading in the laboratory. The load is applied proportionally by ABAQUS/CAE to simulate the actual load increase.

3.5. Solution Algorithm. An appropriate incremental-iterative procedure was adopted to solve the nonlinear equations. The vertical loads were applied as pressure load as it is the most convenient and close to the loading condition in the laboratory, and for each increment, general static analysis step was implemented with 1 second of time and 0.01 as initial increment. Convergence was successfully achieved at the end of each load step using this procedure.

4. Experimental Program

4.1. Description of Specimens. For this research, four beams with dimensions of 150 mm \times 300 mm \times 2300 mm, as shown in Table 1, were fabricated. The beams were grouped into group CB (control beam) and group BSC (beam steel plate with connector). Group CB consisted of one control beam.

Group BSC consisted of three beams, which were BSC20, BSC25, and BSC30. The width of the shear strip plates was selected based on the proposed theoretical models. Beams BSC20 and BSC30 were designed based on tensile and yield strength of shear link as per (12) and (10), respectively, and designed widths of plates were 20 mm and 30 mm, respectively. Beam BSC25 was prepared based on arbitrary basis, and the width of the plate was 25 mm. The thickness of all strengthening plates was 2.75 mm. The embedded connector system was applied with a hole of 20 mm, 25 mm, and 30 mm diameter, respectively, and steel bars with diameters of 16 mm, 16 mm, and 20 mm were inserted into the holes, respectively, in order to eliminate premature debonding failure. The details of all beam specimens are shown in Table 1.

4.2. Properties of Materials. The concrete cube compressive strength used for the casting of beams was 31.385 MPa. A 16 mm steel bar was used for main reinforcement with yield strength of 548 MPa and tensile strength of 620 MPa, while 6 mm bar was used for shear link with yield strength of 305 MPa and tensile strength of 458 MPa. Steel plates with yield strength of 275 MPa and tensile strength of 320 MPa were used for shear strengthening.

4.3. Preparation of Beam Specimens

4.3.1. Casting of Beams. All beams were casted continuously from the same ready mixture patch of grade 32 using oiled wooden molds with proper vibration to avoid honeycomb. The concrete patch was tested on slump test, and cubes, cylinders, and prism samples were casted for further tests of concrete strength.

4.3.2. Shear Strengthening

(1) Surface preparation. The surface of the beam was roughened in the targeted areas to remove the weak concrete

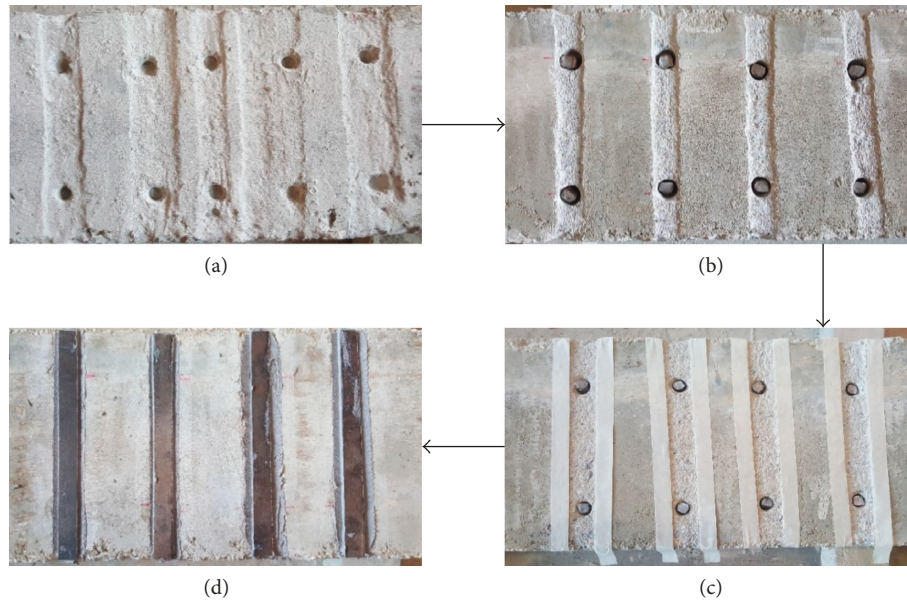


FIGURE 2: Shear strengthening of RC beam using steel plate and embedded connector: (a) surface preparation with hole of connector; (b) embedded connector; (c) prepared surface and connector for strengthening; (d) shear-strengthened beam.

cover and loose particles in order to apply the adhesive on a concrete surface with sufficient strength as the concrete cover would fail at low loads (Figure 2(a)).

(2) *Embedded connector.* In connector system, two holes with a depth of 21–24 mm and the specified diameter were drilled in the roughened area of each steel plate at the distance of 50 mm from the lower and upper edges of the beam. Epoxy resin (Sikadur-30) was used to fill the holes of the connectors, and then, pieces of steel bars of the specified diameter as shown in Table 1 and 21 mm–24 mm in length were placed into the adhesive-filled drilled holes.

(3) *Shear strengthening.* Steel plates were fixed on the sides of the beams by epoxy resin and embedded connector system. The epoxy resin was spread in 3 mm layer over the roughened area on the concrete beam, and the steel plate was applied with firm pressure to ensure proper bonding with no air voids. Epoxy resin was left until it completely dried out, and disruption was avoided (Figure 2).

4.3.3. *Instrumentation and Test Setup.* Strain gauges of 30 mm length were installed on the main reinforcement bars and the top concrete surface at the middle of the beam. Two of the shear links and steel plates in the shear zone were fixed with strain gauges of 10 mm in length. All beams were tested on shear by applying four-point loading with 2000 mm between supports and 550 mm shear span. The dimensions of the testing procedure are shown in Figure 3. The loading of the beams was applied by manually operated hydraulic jack where the pressure was increased steadily and slowly till the failure of the beam. The data were

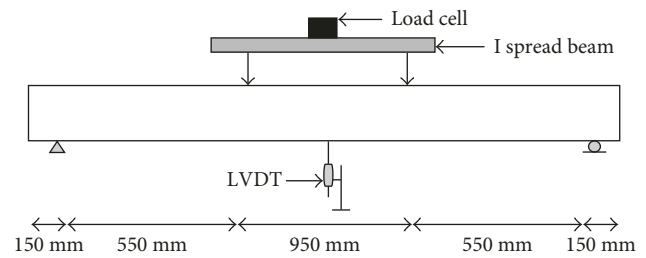


FIGURE 3: Test setup.

recorded using data logger with a rate of 10–15 readings per minute.

5. Experimental Results of Various Shear-Strengthened Beams with Connectors

Extensive data on the strength, deformation, and failure characteristics of the nonstrengthened and strengthened beams were obtained and discussed in three subsequent sections in terms of the observed mode of failure, failure load, and optimization of steel plate.

5.1. *Modes of Failures.* The unstrengthened control beam failed in shear mode by yielding of shear link since it was designed to fail by shear as shown in Figure 4(a), while beams BSC20 and BSC25 failed due to embedded connector and debonding of the externally bonded steel plates at adhesive-plate interface as shown in Figures 4(b) and 4(c), respectively. Both beams showed debonding of plates at plate-adhesive interface rather than concrete-adhesive interface. Embedded connectors prevented debonding of plates at concrete-adhesive interface. However, connectors could not prevent debonding of plates at plate-adhesive interface. It was also noticed that the

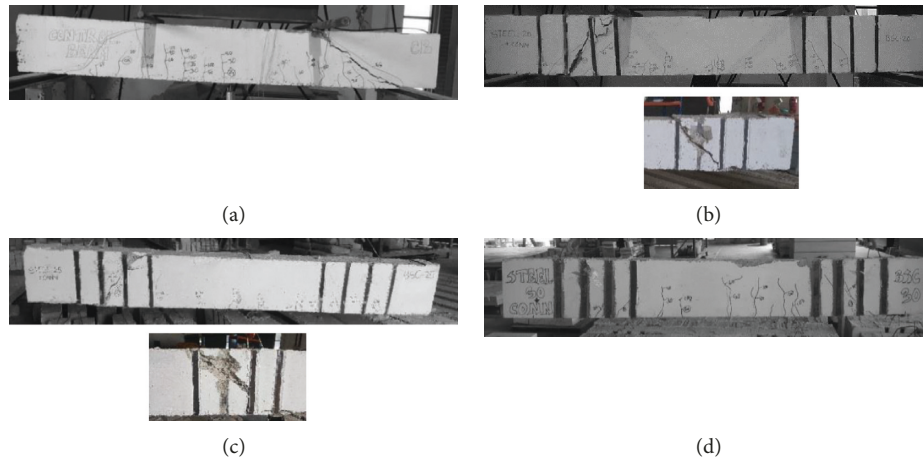


FIGURE 4: Experimental failure mode of beams (a) CB, (b) BSC20, (c) BSC25, and (d) BSC30.

TABLE 2: Experimental results.

Specimen	Failure load (kN)	Strain (micro) at maximum load				Deflection (mm) at maximum kN load	First flexural crack load (kN)	First shear crack load (kN)	Debonding load (kN)	Mode of failure
		Flexural (μ)	Shear (μ)	Laminate (μ)	Concrete compressive (μ)					
CB	155.9	3275	9166	—	2445	11.54	24	55	155.9	Shear
BSC20	178.6	2582	852	244	515	11.79	22	77	178.6	Debonding on adhesive-plate interface
BSC25	189.6	2895	345	102	319	12.01	23	73	189.6	Debonding on adhesive-plate interface
BSC30	193.4	2437	1577	758	2475	11.43	24	75	193.4	Flexure

shear damage on beam BSC20 was more severe than that on BSC25, which indicated that the increase in plate width assisted to control the crack propagation of the beam. In addition, beam BSC20 showed a brittle failure behavior as cracks opened widely, while beam BSC25 was more ductile.

In beam BSC30, although shear cracks were observed, debonding did not occur and it failed by flexure as shown in Figure 4(d). The failure mode of the beam was found to be ductile in nature, and no wide cracks appeared near midspan of beam as shown in Figure 4(d). Embedded connectors prevented debonding of plate at concrete-adhesive interface, and because of sufficient bonding area, plate also did not debond at plate-adhesive interface, and thus, the system completely prevented premature debonding of plate, whereas the bonding area in beams BSC20 and BSC25 was insufficient to prevent adhesive-plate debonding failure at the location of the connector, which might be due to excessive stresses at plate-adhesive interface; thus, the beams showed debonding failures of plates at plate-adhesive interface.

5.2. Failure Load. As shown in the results in Table 2, the steel plate-strengthened beams BSC20, BSC25, and BSC30 failed at 178.6 kN, 189.6 kN, and 193.4 kN, respectively, while the control beam failed at 155.9 kN. There was an increase in failure load of 14.5%, 21.6%, and 24% for beams BSC20,

BSC25, and BSC30, respectively, in comparison with control beam. The steel plate-strengthened beams showed a regular increase in failure load with the increase in steel plate width. This indicated that the width of the steel plate had a great effect on the shear capacity of the strengthened beam. The bigger width of the plate meant larger bonding area and lower chance of debonding failure.

5.3. Optimization of Steel Plates. As observed in the results of this research, failure load increased as the width of the plates increased. Yet, beams BSC20 and BSC25 failed on shear as debonding failure occurred at the adhesive-plate interface, while beam BSC30 failed on flexure and no debonding was observed. Thus, beam BSC30 had higher shear capacity as compared to others. The ductility of beam BSC30 was found to be higher as shown in Figure 5(a), since the flexural reinforcements of the beam had yielded before failure (Figure 5(b)). Amongst all strengthened beams, the shear reinforcement of BSC30 had shown higher strain and it is almost close to the yield strain which resulted in the optimal use of the reinforcement as shown in Figure 5(c). The strain of plate of BSC30 had also found to be higher, which also resulted in the optimal use of steel plate as shown in Figure 5(d). Therefore, steel plate with a 30 mm width seems to be the most effective in the proposed shear strengthening system of

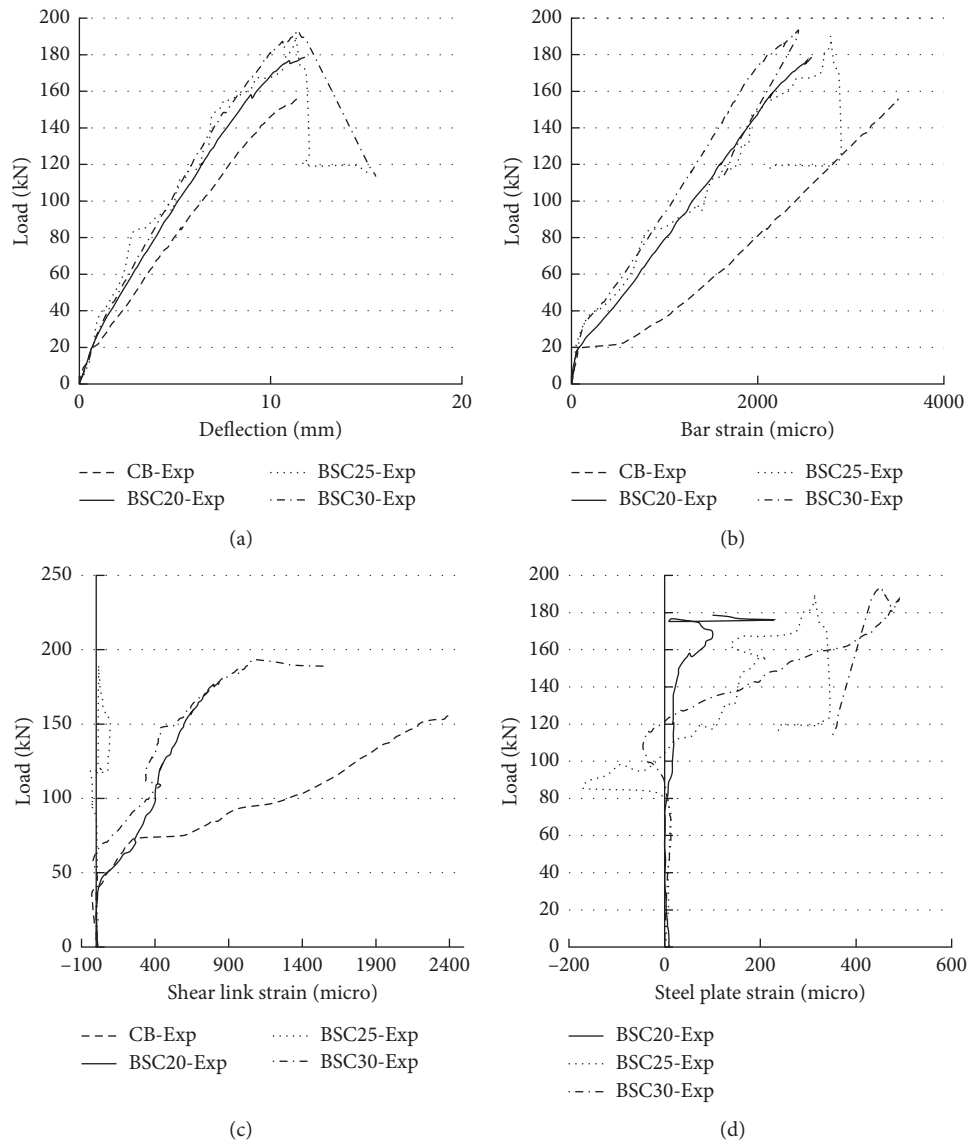


FIGURE 5: Experimental results on optimal shear-strengthened beam plate: (a) experimental deflection of beams; (b) experimental strain of flexural bar; (c) experimental strain of shear link; (d) experimental strain of steel plate.

RC beam using steel plate. Thus, proposed design considering yielding of shear link would be the optimal design method of shear strengthening of RC beam using the existing embedded connector system. However, plate width could be further reduced, and the proposed optimal design considering tensile strength of shear link would be used if the debonding at adhesive-plate interface could be prevented. Furthermore, a beam with different dimensions or steel reinforcements might have different optimal steel plate width, and thus, more research is needed.

6. Comparison of Numerical and Experimental Results

6.1. Comparisons of Failure Modes. The numerical analysis predicted the shear stresses of control and shear-strengthened beams as shown in Figure 6. The highest

shear stress pattern of control beam as shown in Figure 6(a) was almost similar trend of experimental shear failure. The shear stresses of all strengthened beams were found to be similar which reflect the experimental shear crack pattern of beams. Numerical results showed that the shear stress concentration of strengthened beams was higher near the externally bonded plates, which could initiate the debonding of plates. It was observed that numerical analysis could not predict debonding failure of externally bonded plates which would reflect the shear failure loads of beams.

6.2. Comparison of Load-Midspan Deflection. The experimental control beam had a failure load that is 16.6% smaller and a midspan displacement at failure that is 32% larger than in the numerical control beam. The slopes of the deflection versus load curves in both cases were seen to be quite similar although the experimental slope was steeper. The beams

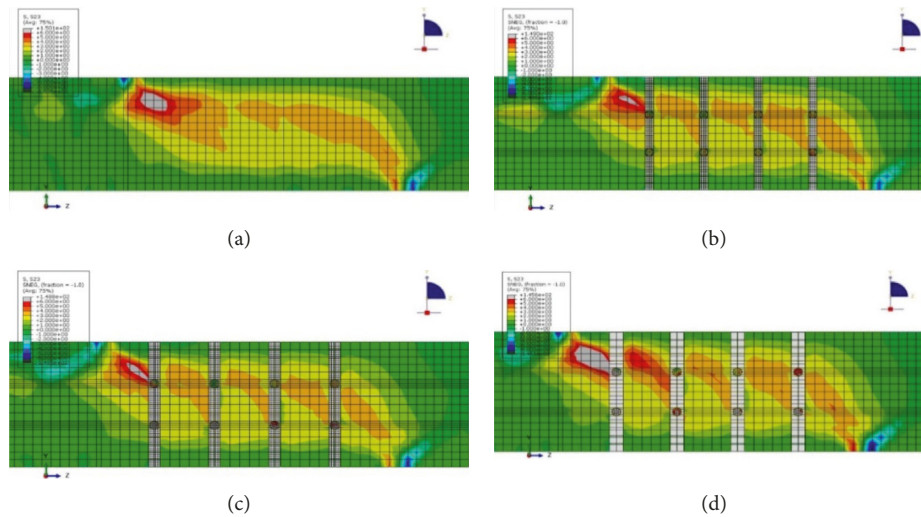


FIGURE 6: Numerical failure mode of beams (a) CB, (b) BSC20, (c) BSC25, and (d) BSC30.

BSC20, BSC25, and BSC30 had failure loads with 2-3% difference between the experimental and the corresponding numerical beams (Table 3). The midspan deflection graphs of the experimental beams were comparable to their corresponding numerical beams where numerical graphs tend to be steeper than the experimental graphs as shown in Figure 7(a), which might be due to the perfect condition of bonding between reinforcement and concrete. It was noticed that the midspan deflections at failure loads of the numerical beams were almost similar for all beams, although failure loads were different.

6.3. Comparison of Main Reinforcement Strain at Midspan. Strain data were retrieved from finite element locations matching the location of the experimental strain gauges. It was noticed that flexural steel strain at failure loads of the experimental beams BSC20, BSC25, and BSC30 was lower than the control beam by 21%, 11%, and 25%, respectively. The experimental values of flexural bar strains of all strengthened beams were found to be higher as compared to the numerical results because concrete stresses were transferred to main reinforcements causing high strains. However, as the strengthening system was sufficient to eliminate debonding of steel plates in beam BSC30 while shear cracks were controlled by strengthening steel plates, which led to flexural failure of beam due to yielding of steel reinforcements followed by crushing of concrete. The experimental graphs of the steel strain were fairly similar to the corresponding numerical graphs Figure 7(b).

6.4. Comparison of Concrete Strain at Midspan. Control beam and beam BSC30 experimental results showed more inclined graphs as concrete cracks occurred early while numerical results did not show any sign of cracks as the tested model was not able to produce concrete cracks. On the other hand, beams BSC20 and BSC25 exhibited

a small sign of concrete cracks where the numerical and experimental data were almost identical as shown in Figure 7(c).

6.5. Comparison of Steel Plate Strain. Strain data for the strengthening steel plates showed similar behavior when compared between numerical and experimental results; however, the numerical strain obtained had smaller values which might be because of the absence of concrete cracks in the numerical model. The strain values would increase when the width of the plate was increasing; nevertheless, the experimental strain value of beam BSC25 appeared to be corrupted due to malfunction of the strain gauge. The maximum plate stain value of experimental beam BSC30 showed an increase of 68% compared to beam BSC20, while numerical strain values of beams BSC25 and BSC30 showed an increase of 37% and 57%, respectively, compared to beam BSC20 as shown in Figure 7(d).

6.6. Comparison of Shear Link Strain. The strains of shear reinforcements obtained from numerical analysis were found to be smaller as compared to experimental findings. It was because of shear cracks, since numerical analysis was unable to cause shear cracks and thus showed smaller strains of shear reinforcements. The maximum experimental stain value of beam BSC30 showed an increase of 46% compared to beam BSC20, while numerical strain values of beams BSC25 and BSC30 showed an increase of 34% and 38%, respectively, compared to beam BSC20 Figure 7(e).

7. Conclusion

Embedded connectors prevented premature debonding of steel plates at concrete-adhesive interface rather than plate-adhesive interface. The embedded connector of shear-strengthened

TABLE 3: Comparisons between numerical and experimental results.

Specimen	Failure load (kN)		Flexural (μ)		Shear (μ)		Strain (micro) at maximum load		Plate (μ)		Concrete compressive (μ)		Deflection (mm) at maximum kN load		First flexural crack load (kN)		First shear crack load (kN)	
	Numerical	Experimental	Numerical	Experimental	Numerical	Experimental	Numerical	Experimental	Numerical	Experimental	Numerical	Experimental	Numerical	Experimental	Numerical	Experimental	Numerical	Experimental
CB	155.9	187	3275	2895	9166	120	—	—	—	—	2445	772	11.54	7.84	24	25.3	55	71
BSC20	178.6	184.8	2582	2836	852	179	244	238	238	515	1080	11.79	8.08	22	25.5	77	77.8	
BSC25	189.6	185.2	2895	2990	345	297	102	297	297	319	1342	12.01	7.76	23	25.6	73	49.3	
BSC30	193.4	188.9	2437	2882	1577	291	758	305	305	2475	788	11.43	8	24	25.6	75	53.3	

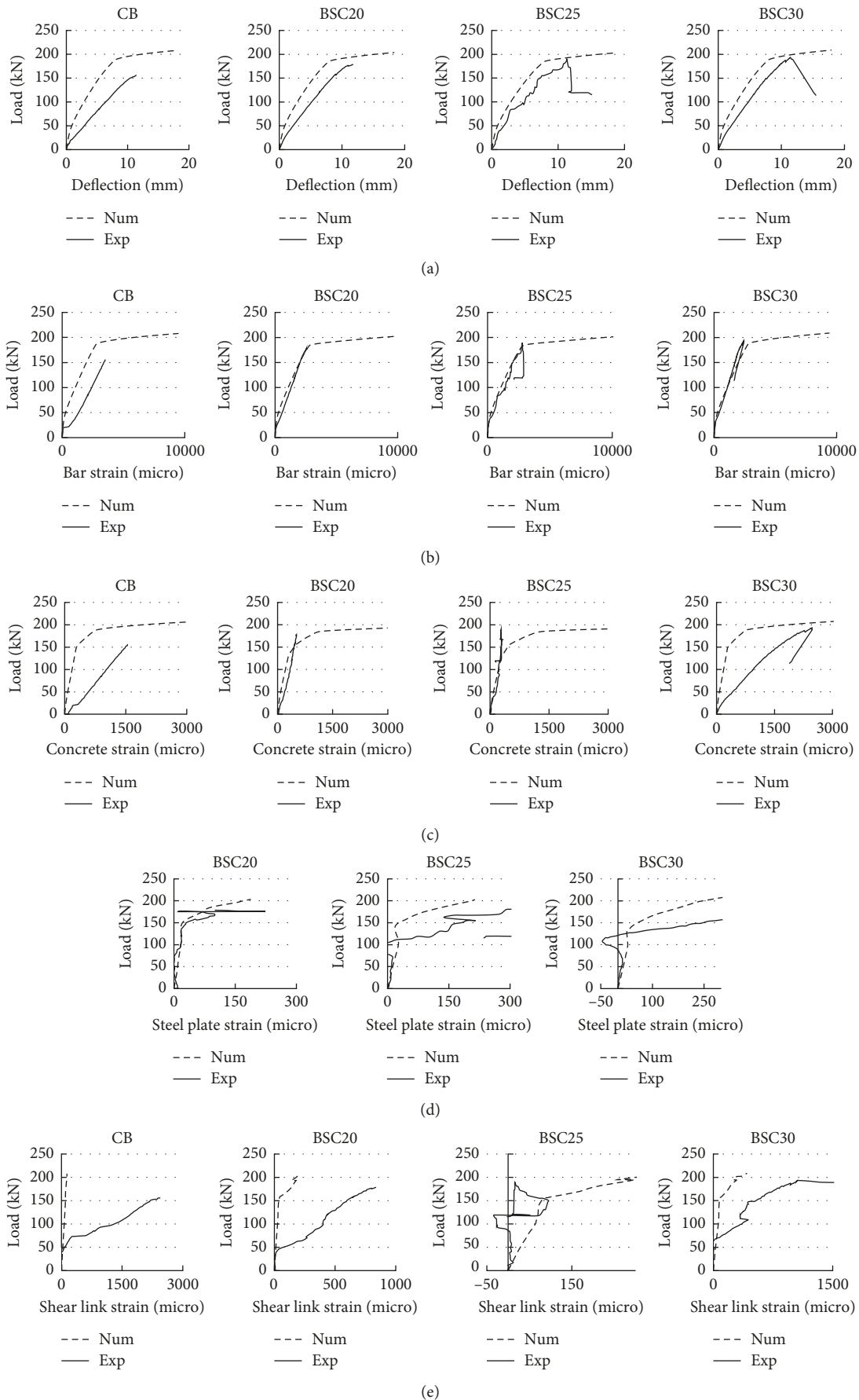


FIGURE 7: Comparison of numerical and experimental results: (a) comparison of numerical and experimental load-midspan deflection; (b) comparison of numerical and experimental flexural reinforcement strain; (c) comparison of numerical and experimental concrete strain at midspan; (d) comparison of numerical and experimental steel plate strain; (e) comparison of numerical and experimental shear link strain.

beam of proposed optimal design based on yielding of shear reinforcement (BSC30) completely prevented debonding of plate and had shown flexural failure with higher failure load and maximum ductile nature.

The bonded area of the plate of beam BSC30 was sufficient to prevent debonding of plate at plate-adhesive interface, whereas strengthened beams having smaller bonded area of plates (BSC25, BSC20) showed failure of connectors and debonding of plates at plate-adhesive interface with lower failure loads and brittle nature of failure. The proposed design model based on yielding of shear reinforcement could be used to optimize the dimension of steel plate for shear strengthening of RC beam.

The collected strain and deflection data from numerical model supported the experimental findings of this research as the results were highly related between the two of them.

At the end, although shear strengthening using embedded connector system is promising, more research is needed to verify the results of this study. Furthermore, it is recommended for future investigations to use different arrangement of steel plates or increase the number of connectors used for single plate, which might help reduce the load carried by each connector.

Nomenclature

V_{\max} :	Maximum shear strength of RC beam
M_{\max} :	Maximum bending moment of RC beam
V_{concrete} :	Shear strength of concrete
V_{plate} :	Shear strength of steel plate
V_{link} :	Shear strength of shear link
V_{beam} :	Shear capacity of beam
$f_{\text{yk,link}}$:	Yield strength of shear link
$f_{\text{tk,link}}$:	Tensile strength of shear link
S_{link} :	Spacing of shear link
$f_{\text{yk,plate}}$:	Yield strength of steel plate
$f_{\text{tk,plate}}$:	Tensile strength of steel plate
S_{plate} :	Spacing of steel plate
w_{plate} :	Width of steel plate
t_{plate} :	Thickness of steel plate
d :	Effective depth of steel bar
d' :	Effective depth of secondary steel bar
ϕ_{link} :	Diameter of shear link
A_{plate} :	Cross-sectional area of steel plate.

Conflicts of Interest

The authors declare that they have no conflicts of interest.

Acknowledgments

The research was conducted in the Department of Civil Engineering, Universiti Tenaga Nasional. The authors would like to express their thanks to the department for the technical and laboratory supports. Thanks are also due to the Innovation & Research Management Centre, iRMC, Universiti Tenaga Nasional, for providing fund under Grant no. J510050677.

References

- [1] A. A. Jamal, S. A. Adi, A. H. Rami, and A. R. Hayder, "Shear strengthening of reinforced concrete beams using externally bonded aluminum alloy plates: An experimental study," *Construction and Building Materials*, vol. 128, pp. 24–37, 2016.
- [2] A. Abu-Obeidah, R. A. Hawileh, and J. A. Abdalla, "Finite element analysis of strengthened RC beams in shear with aluminum plates," *Computers and Structures*, vol. 147, pp. 36–46, 2015.
- [3] K. C. Panda, S. K. Bhattacharyya, and S. V. Barai, "Shear strengthening effect by bonded GFRP strips and transverse steel on RC T-beams," *Structural Engineering and Mechanics*, vol. 47, no. 1, pp. 75–98, 2013.
- [4] W. Li and C. K. Y. Leung, "Shear span–depth ratio effect on behavior of RC beam shear strengthened with full-wrapping FRP strip," *Journal of Composites for Construction*, vol. 20, no. 3, p. 04015067, 2016.
- [5] A. B. Shuraim, "Efficacy of CFRP configurations for shear of RC beams: experimental and NLFE," *Structural Engineering and Mechanics*, vol. 39, no. 3, pp. 361–382, 2011.
- [6] T. C. Triantafillou and C. P. Antonopoulos, "Design of concrete flexural members strengthened in shear with FRP," *Journal of Composites for Construction*, vol. 4, no. 4, pp. 198–205, 2000.
- [7] B. B. Adhikary and H. Mutsuyoshi, "Shear strengthening of reinforced concrete beams using various techniques," *Construction and Building Materials*, vol. 20, no. 6, pp. 366–373, 2006.
- [8] Ö. Anil, N. Bulut, and M. Ayhan, "Strain distribution between CFRP strip and concrete at strengthened RC beam against shear," *Structural Engineering and Mechanics*, vol. 41, no. 4, pp. 509–525, 2012.
- [9] L. Ascione and L. Feo, "Modeling of composite/concrete interface of RC beams strengthened with composite laminates," *Composites Part B: Engineering*, vol. 31, no. 6-7, pp. 535–540, 2000.
- [10] D. Baggio, K. Soudki, and M. Noël, "Strengthening of shear critical RC beams with various FRP systems," *Construction and Building Material*, vol. 66, pp. 634–644, 2014.
- [11] H. N. Garden and L. C. Hollaway, "An experimental study of the failure modes of RC beams strengthened with prestressed carbon composite plates," *Composites Part B: Engineering*, vol. 29, no. 4, pp. 411–424, 1998.
- [12] J. Sim, C. Park, and D. Y. Moon, "Characteristics of basalt fiber as a strengthening material for concrete structures," *Composites Part B: Engineering*, vol. 36, no. 6-7, pp. 504–512, 2005.
- [13] B. Taljsten and L. Elfgren, "Strengthening of concrete beams for shear using CFRP materials: evaluation of different application methods," *Composites Part B: Engineering*, vol. 32, no. 2, pp. 87–96, 2000.
- [14] J. Yao, J. G. Teng, and J. F. Chen, "Experimental study on FRP-to-concrete bonded joints," *Composites Part B: Engineering*, vol. 36, no. 2, pp. 99–113, 2005.
- [15] I. A. Bukhari, R. L. Vollum, S. Ahmad, and J. Sagaseta, "Shear strengthening of reinforced concrete beams with CFRP," *Magazine of Concrete Research*, vol. 62, no. 1, pp. 65–77, 2010.
- [16] S. Y. Cao, J. F. Chen, J. Teng, Z. Hao, and J. Chen, "Debonding in RC beams shear-strengthened with complete FRP wraps," *Journal of Composites for Construction*, vol. 9, no. 5, pp. 417–428, 2005.

- [17] A. Carolin and B. Täljsten, "Experimental study of strengthening for increases shear bearing capacity," *Journal of Composites for Construction*, vol. 9, no. 6, pp. 488–496, 2005.
- [18] A. Carolin and B. Täljsten, "Theoretical study of strengthening for increased shear bearing capacity," *Journal of Composites for Construction*, vol. 9, no. 6, pp. 497–506, 2005.
- [19] G. M. Chen, *Behaviour and Strength of RC Beams Shear-strengthened with Externally Bonded FRP Reinforcement*, Ph.D. thesis, Hong Kong Polytechnic University, Hong Kong, 2010.
- [20] A. Bouselham and O. Chaallal, "Mechanisms of shear resistance of concrete beams strengthened in shear with externally bonded FRP," *Journal of Composites for Construction*, vol. 12, no. 5, pp. 499–512, 2008.
- [21] O. Chaallal, M. Shahawy, and M. Hassan, "Performance of reinforced concrete T-girders strengthened in shear with carbon fiber-reinforced polymer fabric," *ACI Structural Journal*, vol. 99, no. 3, pp. 335–343, 2002.
- [22] J. F. Chen and J. G. Teng, "Shear capacity of FRP-strengthened RC beams: FRP debonding," *Construction and Building Materials*, vol. 17, no. 1, pp. 27–41, 2003.
- [23] G. M. Chen, J. G. Teng, J. F. Chen, and O. A. Rosenboom, "Interaction between steel stirrups and shear-strengthening FRP strips in RC beams," *Journal of Composites for Construction*, vol. 14, no. 5, pp. 498–509, 2010.
- [24] G. M. Chen, J. G. Teng, and J. F. Chen, "Shear strength model for FRP-strengthened RC beams with adverse FRP-steel interaction," *Journal of Composites for Construction*, vol. 17, no. 1, pp. 50–66, 2012.
- [25] J. Jayaprakash, A. A. A. Samad, A. A. Abbasovich, and A. A. A. Ali, "Repair of precracked RC rectangular shear beams using CFRP strip technique," *Structural Engineering and Mechanics*, vol. 26, no. 4, pp. 427–439, 2007.
- [26] A. Khalifa and A. Nanni, "Improving shear capacity of existing RC T-section beams using CFRP composites," *Cement and Concrete Composites*, vol. 22, no. 3, pp. 164–174, 2000.
- [27] S. J. Kim and S. T. Smith, *Shear Strength and Behaviour of FRP Spike Anchors in Cracked Concrete*, ICE Australia, Sydney, Australia, 2009.
- [28] S. L. Orton, J. O. Jirsa, and O. Bayrak, "Design considerations of carbon fiber anchors," *Journal of Composites for Construction*, vol. 12, no. 6, pp. 608–616, 2008.
- [29] K. T. Quinn, *Shear Strength of Reinforced Concrete Beams with Carbon Fiber Reinforced Polymer (CFRP) and Improved Anchor Details*, University of Texas at Austin, Austin, TX, USA, 2009.
- [30] S. T. Smith and S. J. Kim, *Shear Strength and Behaviour of FRP Spike Anchors in FRP-to Concrete Joint Assemblies*, Multi Science Publ. Co. Ltd., Winnipeg, Canada, 2008.
- [31] M. A. Alam, W. Mohammed, S. Bakkar, and S. Beddu, "Prevention of premature failures of plate bonded flexurally strengthened RC slab using end anchor and connector," *Alexandria Engineering Journal*, vol. 57, no. 1, pp. 287–299, 2018.
- [32] G. El-Saikaly, A. Godat, and O. Chaallal, "New anchorage technique for FRP shear-strengthened RC T-beams using CFRP rope," *Journal of Composites for Construction*, vol. 19, no. 4, p. 04014064, 2015.
- [33] G. M. Chen, Z. Zhang, Y. Li, X. Q. Li, and C. Y. Zhou, "T-section RC beams shear-strengthened with anchored CFRP U-strips," *Composite Structures*, vol. 144, pp. 57–79, 2016.
- [34] Z. C. Tetta, L. N. Koutas, and D. A. Bournas, "Shear strengthening of full-scale RC T-beams using textile-reinforced mortar and textile-based anchors," *Composites Part B: Engineering*, vol. 95, pp. 225–239, 2016.
- [35] N. H. Ammar, M. S. Jaafar, H. Farzad, and N. A. A. Farah, "Strut-and-tie model for externally bonded CFRP-strengthened reinforced concrete deep beams based on particle swarm optimization algorithm: CFRP debonding and rupture," *Construction and Building Materials*, vol. 147, pp. 428–447, 2017.
- [36] ACI Committee 440, *Guide for the Design and Construction of Externally Bonded FRP Systems for Strengthening Concrete Structures*, ACI 440, Farmington Hills, MI, USA, 2002.
- [37] M. A. Alam, S. Ali, and N. M. Kamal, "Embedded connectors to eliminate debonding of steel plate for optimal shear strengthening of RC beam," *Arabian Journal for Science and Engineering*, vol. 42, no. 9, pp. 4053–4068, 2017.
- [38] ACI-440, ACI 440.1R-06, *Guide for the Design and Construction of Structural Concrete Reinforced with FRP Bars*, American Concrete Institute, Farmington Hills, MI, USA, 2006.
- [39] K. S. Panigrahi, A. Deb, and K. S. Bhattacharyya, "Modes of failure in shear deficient RC T-beams strengthened with FRP," *Journal of Composites for Construction*, vol. 20, no. 1, p. 04015029, 2016.
- [40] H. Baghi and J. A. O. Barros, "Shear strengthening of reinforced concrete T-beams with hybrid composite plate," *Journal of Composites for Construction*, vol. 20, no. 6, p. 04016036, 2016.
- [41] U. Khan, M. A. Al-Osta, and A. Ibrahim, "Modeling shear behavior of reinforced concrete beams strengthened with externally bonded CFRP sheets," *Structural Engineering and Mechanics*, vol. 61, no. 1, pp. 125–142, 2017.
- [42] H. K. Lee, S. K. Ha, and M. Afzal, "Finite element analysis of shear-deficient RC beams strengthened with CFRP strips/sheets," *Structural Engineering and Mechanics*, vol. 30, no. 2, pp. 247–261, 2008.
- [43] O. Awani, T. El-Maaddawy, and A. El Refai, "Numerical simulation and experimental testing of concrete beams strengthened in shear with fabric-reinforced cementitious matrix," *Journal of Composites for Construction*, vol. 20, no. 6, p. 04016056, 2016.
- [44] *Abaqus/CAE 6.9 Finite Element Analysis Software [Computer Software]*, Dassault Systemes Simulia, Waltham, MA, USA.
- [45] P. J. Firmo, T. R. M. Arruda, R. J. Correia, and C. I. Rosa, "Three-dimensional finite element modelling of the fire behaviour of insulated RC beams strengthened with EBR and NSM CFRP strips," *Composite Structures*, vol. 183, pp. 124–136, 2017.



Hindawi

Submit your manuscripts at
www.hindawi.com

